ARTICLE

BIOTECHNOLOGY and BIOENGINEERING

Enhanced Cell Viability Via Strain Stimulus and Fluid Flow in Magnetically Actuated Scaffolds

Julia J. Mack,[1] Abigail A. Corrin,[1,2] Sergio L. dos Santos e Lucato,[1] James C.Y. Dunn,[2] Benjamin W. Wu,[2] Brian N. Cox[1]

[1]Teledyne Scientific Co. LLC, 1049 Camino Dos Rios, Thousand Oaks, California 91360; telephone: (805) 373-4128; fax: (805) 373-4775; e-mail: bcox@teledyne.com

[2]Department of Bioengineering, University of California, Los Angeles, California 90095

ABSTRACT: A novel magnetically actuated scaffold was used to explore the effects of strain stimulus on the proliferation and spatial distribution of smooth muscle cells and improve cell viability in the scaffold interior by pumping nutrients throughout the structure. Magnetically actuable scaffolds were fabricated in a tube shape by winding electrospun sheets of a biodegradable polymer modified with magnetic Fe_2O_3 nanoparticles. Prior to rolling, the sheets were seeded with smooth muscle cells and wound into tubes with diameter 5.2 mm and wall thickness 0.2 mm. The tubular scaffolds were actuated by a magnetic field to induce a cyclic crimping deformation, which applies strain stimulus to the cells and pumps nutrient fluid through the porous tube walls. Comparison with non-actuated controls shows that magnetic actuation increases the total cell count throughout the scaffold after 14 days of incubation. Furthermore, whereas cell density as a function of position through the tube wall thickness showed a minimum in the mid-interior in the controls after 14 days due to cell starvation, the actuated scaffolds displayed a maximum cell density. Comparison of cell distributions with the expected spatial variations in strain amplitude and nutrient flux implies that both strain stimulus and nutrient pumping are significant factors in cell proliferation.

Biotechnol. Bioeng. 2013;110: 936–946.

KEYWORDS: magnetic actuation; 3D scaffold; strain stimulus; nutrient pumping

Introduction

Porous polymeric scaffolds are often used as a three-dimensional (3D) structure to support cell growth in culture (Griffith and Naughton, 2004). However, cell growth within a 3D scaffold is limited by the diffusion of nutrients through the thickness and therefore tissues grown in vitro under static culture are less than 1 mm in thickness (Lee et al., 2008). Another limitation is consumption of nutrients by peripheral cells residing closer to the surface of the scaffold (Galban and Locke, 1999). Due to lack of diffusion and the consumption of oxygen and nutrients by cells at the fluid–scaffold interface, cell growth in the interior of the scaffold is inhibited. This results in a gradient of cell density through the scaffold with the highest population of cells near the scaffold exterior. For cell growth in 5 mm thick demineralized bone matrix, oxygen concentrations dropped to ~0% in the center of the cell-seeded scaffolds in 5 days under static culture conditions; and after 7 days, only cells on the periphery of the scaffold (top and side) remained viable (Volkmer et al., 2008). Further investigations in 3D culture of osteoblasts in porous PLGA scaffolds found that mineralized penetration depth and total cell count were independent of the scaffold thickness; only the outer 200 microns contained viable cells and mineralized tissue after 56 days (Ishaug-Riley et al., 1998).

Bioreactors provide a controlled environment by which biochemical and physical stimulation can be applied to cell cultures in vitro (Abousleiman and Sikavitsas, 2006), possibly overcoming limitations on cell growth and aiding in the development of functional tissue (Freed et al., 2006). Bioreactor systems have utilized flow to apply shear stress and improve mass transport (Dennis et al., 2009). Perfusion bioreactors have been used to improve convection of nutrients and minimize diffusion constraints through the scaffold (Carrier et al., 2002). Researchers have used a flow perfusion bioreactor to pump medium through a porous PLLA scaffold and thereby enhance delivery of nutrients as well as provide mechanical stimulation to marrow stromal cells, which increased calcium deposition (Sikavitsas et al., 2005). The shortcoming of bioreactor technology is the inability to translate to in vivo use.

Clinical applications of engineered tissues grown in vitro have shown viable cells post implantation yet limitations still remain to achieve functional tissue. Researchers have demonstrated tracheal transplantation of a tissue grown within a double-chamber rotating bioreactor. Although transplantation was successful with viable chondrocytes and

Correspondence to: Brian N. Cox
Contract grant sponsor: National Institute of Biomedical Imaging and Bioengineering
Contract grant number: R21EB003900
Additional supporting information may be found in the online version of this article.
Received 4 June 2012; Revision received 10 August 2012; Accepted 17 September 2012
Accepted manuscript online 5 October 2012;
Article first published online 11 October 2012 in Wiley Online Library (http://onlinelibrary.wiley.com/doi/10.1002/bit.24736/abstract)
DOI 10.1002/bit.24736

epithelial cells 2 months post-surgery, the epithelial layer was found to be microscopically discontinuous resulting in inefficient clearance of mucus (Asnaghi et al., 2009). As a general finding, specific tissues can be grown in vitro using bioreactors; however once implanted in vivo, a tissue greater than 2–3 mm^3 cannot survive due to the large cell mass (Shieh and Vacanti, 2005). In order to develop a system to apply convection in vivo, there is a need for a remotely actuated system. Several groups have used magnetic nanoparticles to achieve remotely triggered release of model drugs in vivo by a magnetically triggered delivery vehicle (Derfus et al., 2007; Hoare et al., 2009; Nikles et al., 2010). Researchers in the field of cardiac tissue engineering have focused on electrical stimulation as a means to improve functional performance. Bioengineers in cardiac research have constructed chambers to apply electrical stimuli via linear electric field gradients to cultured cardiomyocytes or adipose-derived stem cells and assess contractile activity (Tandon et al., 2010, 2011). While bioreactor technology has advanced to incorporate mechanical and electrical stimuli to cell-seeded scaffolds, currently there are no reports of scaffold materials which can be actuated via a non-contact mechanism.

In this work, we demonstrate non-contact actuation of a 3D magnetically functionalized polymeric scaffold in vitro to sustain cell growth and encourage cell proliferation. The novelty of this approach lies in its providing a potential method of stimulating an implanted scaffold in vivo using externally applied fields. Our previously published work demonstrates the ability to incorporate magnetic nanoparticles within a biocompatible polymer via electrostatic spinning. Magnetic γ-Fe_2O_3 nanoparticles are embedded and dispersed within polyglycolide–polycaprolactone nanofibers. The resulting magnetic fibrillar sheet can then be wound into a tubular structure and induced to deform under an external magnetic field. The deformation creates strains and fluid pumping radially through the tube walls (Mack et al., 2009).

In this article, we expand our previous study to test the hypothesis that magnetic actuation of our scaffold system can promote the proliferation of cells in vitro. The magnetically functionalized electrospun sheets are seeded with rat aortic smooth muscle cells and subsequently wound into a multi-layered tubular structure, such that the cells are contained within the tube walls. The magnetic actuation of the tube enables nutrient pumping through the porous walls and sustains cell growth. The benefit of actuation is tested by comparing the growth of cells in actuated and non-actuated scaffold systems for periods up to 15 days.

Materials and Methods

Materials

Polycaprolactone (PCL) was purchased from Durect Corporation (Cupertino, CA) and hexafluoroisopropanol (HFIP) was obtained from Sigma–Aldrich (St. Louis, MO). Monocryl sutures were obtained from Ethicon (Johnson & Johnson, Cincinnati, OH). Dulbecco Modified Eagle Medium (DMEM) without phenol red, Fetal Bovine Serum (FBS), Dulbecco's Phosphate-Buffered Saline (DPBS), Calcein-AM, Hoechst-33342 and Goat Anti-mouse with AlexaFluor 488 were purchased from Invitrogen (Carlsbad, CA). Mouse Anti-Collagen I was obtained from Abcam (Cambridge, MA). Rat aorta smooth muscle cells, A7r5 cells, were obtained from the American Type Tissue Culture Collection (Manassas, VA). Neodymium iron boride (NdFeB) magnets, grade N50, 25 mm in diameter and 12.5 mm thick, were purchased from K&J Magnetics, Inc. (Plumsteadville, PA).

Preparation of Magnetic Fibril Sheets

Magnetic fibril sheets were formed by electrospinning within a biodegradable 50/50 blend of polyglycolide (PG) and polycaprolactone (PCL) in which were dispersed magnetic γ-Fe_2O_3 nanoparticles. Sheets with an average thickness of 23 μm were formed and cut to 65 mm by 65 mm dimensions. Further details appear in Appendix A in Supporting Information.

Fibril Sheet Characterization

The overall morphology and average fiber diameter were determined via scanning electron microscopy (SEM) analysis. The average fiber diameter for each sheet ranged from 200 to 400 nm as shown in Figure 1A. The nanofiber mesh provides a large surface area to volume ratio and the interconnected porosity between fibrils provides permeability to facilitate nutrient flow. The magnetic nanoparticles are embedded within the polymer fibers and uniformly dispersed as imaged via transmission electron microscopy (TEM) and shown in Figure 1B. The thickness of the sheets was determined using interference optical microscopy, yielding consistent values of 22 ± 2 μm. Young's modulus

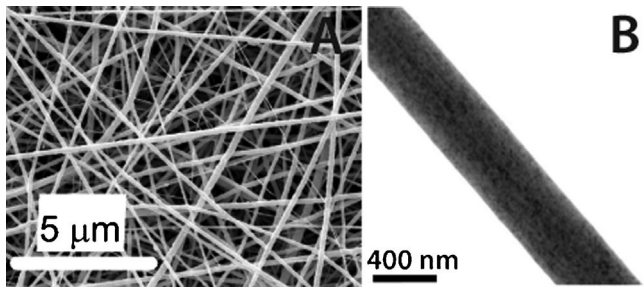

Figure 1. **A**: SEM images of 50 wt % γ-Fe_2O_3/PG-PCL electrospun sheets with average fiber diameter 315 nm. **B**: TEM image showing the distribution of γ-Fe_2O_3 nanoparticles (dark contrast) in electrospun PG-PCL fibers, for a loading of magnetic nanoparticles of 20 weight percent. Because the imaging is made in transmission, dark areas represent the integral of particles through the thickness of the fibril. The distribution is very uniform.

for the sheet material is 1.5 MPa and permeability varied in the range of 2×10^{-15}–10^{-14} m^2 (Mack et al., 2009).

Magnetic hysteresis measurements demonstrated that the γ-Fe_2O_3 nanoparticles exist in a superparamagnetic state in the γ-Fe_2O_3/PG-PCL composite and for magnetic field strengths generated in scaffolds by the actuation system (3–5 kG; Fig. 11 of Mack et al., 2009), the magnetization is saturated (Fig. 10 of Mack et al., 2009). For typical electrospun sheets with 50% mass fraction of Fe_2O_3, such as those used here, the saturation magnetization, μ_{sat}, is approximately 2,300 A/m. When approached by a permanent magnet, the composite experiences body forces, F_m, distributed approximately uniformly through its volume and proportional to the magnetic field gradient

$$F_m = \mu_{sat} \cdot \frac{dB}{dy} \quad (1)$$

where B is the magnetic field and y is the distance of the magnet (Craik, 1995; Jiles, 1991). For the same material composition, $|F_m| = 1.0 \times 10^{-4}$ N/mm^3 (Mack et al., 2009).

Cell Culture and Seeding

Rat aortic smooth muscle cells were grown in low-glucose DMEM supplemented without phenol red supplemented with 10% FBS and ABAM in an incubator with 5% CO_2 maintained at 37°C. Passage 12 or 13 cells were trypsinized and counted with a hemacytometer. The electrospun sheets were disinfected in 70% ethanol (three washes) followed by two washes in DPBS. Once washed, the fibril sheet was soaked in media with serum for 30 min in a large (85 mm diameter) culture dish. After soaking, cells were suspended in serum containing media and pipetted onto the sheet to achieve a cell density of 1,000 mm^{-2} and then incubated for 1 h to initiate cell attachment onto the fibrous sheet. Media with serum was then added and the cells were allowed to attach undisturbed for another hour.

Tubular Scaffold Formation

After cell attachment, the sheets were rolled into tubes using a pair of 4.8 mm diameter (20 mm long) Teflon mandrels (the "Teflon rods" in Fig. 2A). Each tube consists of approximately four cell-fibril layers in a continuous helical winding. Rolling was performed with the cell-seeded side of the sheet in contact with the mandrel. Therefore, the wound tube initially has cells only on the inward-facing surface of each of layer in the helical winding. Once wound, the mandrels were separated to the tube ends to produce an unsupported length of 45 mm. The mandrels are left at the ends of the tube to provide a seal against fluid flow through the ends, thus ensuring that deformation is accompanied by fluid flow through the walls of the tube. The tube was then transferred to an 85 mm diameter culture dish and held in place by a 1.5 mm thick polycarbonate bridge (80 mm long) with two notches drilled in the ends of the bridge to hold the Teflon rods in place, as shown in Figure 2A. Growth medium was added to the dish and then incubated at 37°C and 5% CO_2 for up to 15 days.

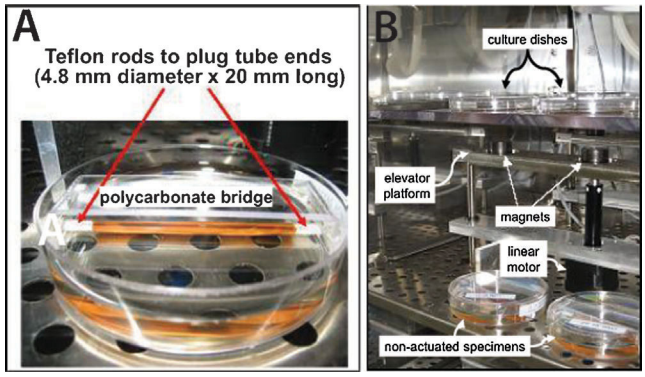

Figure 2. **A**: Wound cell-seeded tubular scaffold (6 cm long, eight wound fibril layers) in a culture dish. **B**: Computer-controlled magnetic elevators in cell culture incubator.

Scaffold Actuation

Permanent magnets mounted on actuators as displayed in Figure 2B were used to apply a cyclically varying magnetic field to each culture. The field gradient causes a crimping deformation of the tube (shown in Fig. 3A), generating bending and shear strains within the wall of the tube, which vary around the circumference of the tube. The magnitudes of the strains vary along the tube length in approximate proportion to the deflection of the crown (see Fig. 3B); the maximum strains induced are several percent, with exact values depending on the details of the displacement field within the tube, which are influenced by shape changes in the tube, buckling modes and possible relative sliding between the layer windings of the tube. The deflection causes the volume enclosed in the tube to decrease and fluid flows through the tube walls, whose permeability governs the rate of change of the deflection. Characteristic times for deflection and recovery are 3–10 seconds (Mack et al., 2009). To ensure adequate time for deflection and recovery, magnetic actuation was cycled for 60 seconds on and 60 seconds off.

The maximum pressure induced in the interior of the tube is approximately $P = 15$ Pa (Appendix B in Supporting Information). This pressure will be the same whether the tubes are cell-laden or cell-free. The flux (fluid flow per unit area per unit time) is given by expressions presented in Appendix B in Supporting Information. The deformation times for a tube are directly related to the fluid flux averaged along the tube. Since the deformation times show no statistically significant variation with elapsed days in culture,

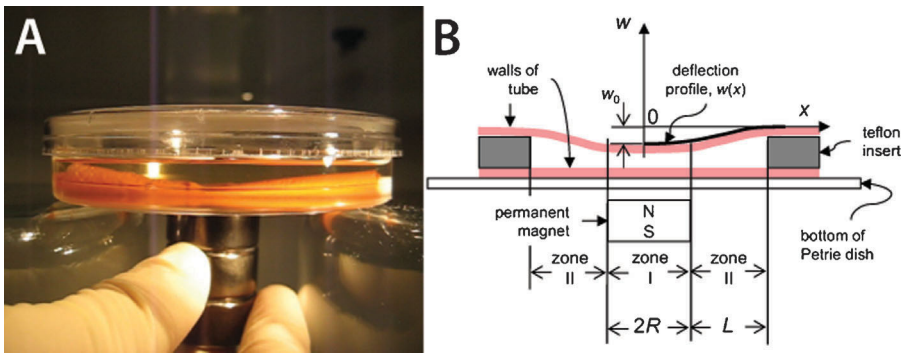

Figure 3. **A**: Wound tube scaffold deflecting down towards the bottom of the culture dish when approached from below by a hand-held permanent magnet. **B**: Schematic of different zones of deflection.

the average permeability of the tube is inferred not to vary significantly even in tests where cells proliferated. However, local permeability may decrease in portions of the tube where cell density is highest; such a change cannot be directly measured.

Scaffolds were incubated for a time period of 1–15 days with the culture medium changed every 3–4 days. For each time period, one scaffold acted as the control (no actuation) and either one or two scaffolds were magnetically actuated for the entire time period. For all scaffolds in each set, the growth medium was changed at the same times. After the set time period, the cell-laden scaffolds were removed, washed with DPBS and unrolled for examination.

Cell Viability Determination

To evaluate cell density and viability, scaffolds were carefully unrolled to minimize tearing or damage, thus exposing the cells that had inhabited the tube walls throughout the wall thickness. Since the magnetically functionalized polymers are opaque, they are not amenable to confocal optical microscopy and conventional sectioning of the tube does not yield information on cell spatial distribution, whereas unrolling provided quantitative cell density data over the entire scaffold. The unrolled tubes were stained and imaged at either 40× or 100× magnification. The side of the sheet that was imaged was the side on which cells were seeded prior to the sheet being rolled into the tube shape. This is also the side facing inwards towards the axis of the tube in its rolled state. The process of unrolling tubes became more difficult when cells proliferated into dense populations, with significant collagen expression.

Because the sheet is opaque, only cells that lie above the sheet or close to the imaged surface appear in images. Therefore, cells that adhered to the underside of an unrolled sheet, as well as cells that were lost during the act of unrolling, are not included in cell counts. The density of viable cells was determined by staining the unrolled cell-laden scaffold with either calcein-AM or Hoechst-33342. For calcein staining, the scaffold was first washed with DPBS, after which staining was done with 2.5 mM calcein-AM. For Hoechst-33342 staining, a solution of 5 μg/mL Hoechst-33342 in serum-free DMEM was used. The stained cells were viewed under a Nikon AZ100 microscope with appropriate filters.

An alternative method of determining cell density values was to fix and embed the scaffold (in paraffin), section into slices and stain. This method did not yield quantitative data on cell densities due to issues with embedding conditions. Furthermore, imaging cross sections does not allow one to determine spatial variations from slice to slice. Unrolling and imaging the exposed surfaces of the entire scaffold sheet enables both a cell count and visualization of cell distributions.

Collagen Assay

To examine collagen type I production, cells on unrolled scaffolds were incubated for 1 h with 2.2 μg/mL anti-mouse anti-collagen I primary antibody. Next, cells were washed with DPBS followed by 1 h incubation with 5 μg/mL of the secondary antibody goat anti-mouse conjugated with AlexaFluor 488 (green fluorescent marker).

Results

Deformation Generated by Magnetic Actuation

The deformation of cell-seeded tube scaffolds was measured from video images and found consistent with measurements on tubes containing no cells (Mack et al., 2009). The tube deflected downwards approximately uniformly above the magnet, that is, in a zone approximately 15 mm long at

the tube's center. The deflection decreased approximately linearly to zero between this zone and the tube ends as outlined in Figure 3B.

The maximum deflection achieved in all cases for which data are reported was approximately one half the tube diameter (deflection = 2.5 mm). For a maximum deflection less than the tube diameter, analysis shows that it is determined by mechanical equilibrium between the magnetic forces, which drive the deflection, and the elasticity of the tube scaffold material, which opposes the deflection (Mack et al., 2009). When the field is removed, the elastic energy stored in the tube causes it to recover its original shape. In the experiments reported, recovery was complete or nearly complete. The tubes deflect consistently over the 1–15 days duration of experiments; thus the stiffness of the material/cell system did not change significantly.

An estimate of the strain distribution in the wall of a tube was made by finite element calculations presented in Appendix C in Supporting Information. The shear strain varies in magnitude around the tube and changes sign at hinge points at the extremities of the tube section (see Supplementary Fig. C.1). It also varies through the wall thickness, at any location, in an approximately parabolic manner with a maximum in the mid-wall region and zero on the inner and outer surfaces as plotted in Figure 4 (Timoshenko and Goodier, 1970). In summary, cells between windings of the tube wall are subjected to cyclic local shear strains during tube collapse and recovery that are at a maximum in the mid-wall region, with peak values in the range 1–5%, depending on whether sliding occurs between the windings.

Radial Fluid Flow Achieved Through Tube Walls

Measurements of deflections and recovery times for all experiments showed that the average permeability of the tube walls had no statistically significant change during experiments (Appendix D in Supporting Information). Further, the fluid pumping action is sufficient to entirely replace the fluid content of the wall interior during each deformation cycle. Thus nutrient pumping is approximately uniform along the tube's length and through the thickness of the tube wall. Details of these deductions are presented in Appendix D in Supporting Information.

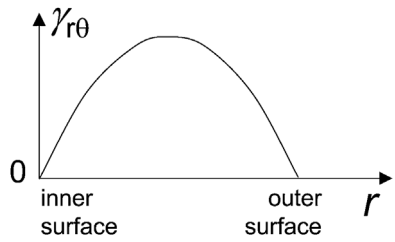

Figure 4. Functional form of shear strain variation through thickness of tube wall is quadratic.

Cell Proliferation

Cell-seeded scaffolds were incubated for between one and 15 days in the presence and absence of magnetic actuation. Scaffolds were unrolled at the conclusion of each experiment to allow direct measurements of cell populations. When unrolled, a single specimen yields significant quantities of data, including trends in cell density and cell spatial distribution versus location along the tube's length and through the thickness of its walls.

Consistent trends were observed in the difficulty of unrolling specimens (Table I). Non-actuated specimens always unrolled with minimal difficulty, whereas actuated specimens were increasingly difficult to unroll with increasing test duration. At 7 days, some damage to the edges of the sheet was inevitable; at 14 days, one specimen was impossible to unroll. These trends correlate with the degree of cell proliferation and ECM production (described later).

Some specimens were stained with calcein-AM, allowing imaging of live cells by fluorescence microscopy and observation of their morphology. For both the control and actuated scaffolds, cells were found to be viable after each time point and exhibited their normal phenotypic shape. Other specimens were analyzed by staining with Hoechst-33342, which images individual cell nuclei and yields more accurate measurements of cell density.

Staining With Calcein-AM

Representative images of actuated and non-actuated scaffolds taken at magnification 40× are shown in

Table I. Qualitative observations of the difficulty of unrolling specimens versus duration of test in days.

Experimental set	Non-actuated	Actuated
Day 1 (set #1)	Easy to unroll	Easy to unroll
Day 1 (set #2)	Easy to unroll	Easy to unroll
Day 7 (set #1)	Unrolled with little manipulation	Required tweezers to unroll
Day 7 (set #2)	Unrolled with little manipulation	Difficult to unroll, multiple edges ripped
Day 10	Unrolled with slight manipulation[a]	Required tweezers and finger force to unroll
Day 14 (set #1)	Unrolled with little manipulation[a]	Very difficult to unroll, use of tweezers and finger force, multiple edges ripped
Day 14 (set #2)	Unrolled with some manipulation[a]	Unable to unroll, ends ripped off

[a]Use of tweezers and gentle pipetting of saline solution.

Supplementary Figure E.1 in Appendix E. Further images taken at 100× are shown in Figure 5 and Supplementary Figure E.2. In all scaffolds, some density of viable cells could be found on the fibril sheet, and for all but the shortest duration tests (1–3 days), the density of cell coverage appears qualitatively greater in actuated compared to non-actuated scaffolds.

By staining with calcein-AM, trends in cell density can be quantified by comparing the percentage of an image that is covered by cells for non-actuated and actuated specimens. The percent coverage was determined for any single image by setting a threshold intensity to flag the presence of cells. The ratio of percent coverage for actuated and non-actuated specimens rose modestly with the test duration up to 7 days, which was the longest test for which calcein-AM staining was used (see Fig. 6A).

Hoecsht-33342 Staining

Figure 7 and Supplementary Figure E.3 show images of the actuated and non-actuated cultures following Hoechst-33342 staining, representative of the mid-wall region. A major qualitative difference is apparent in the cell densities for the actuated and non-actuated cases. To determine a cell count, the Nikon Elements Basic software package was used in Object Count mode. The number of cells (represented by cell nuclei) was counted from a series of images taken along both directions of the unrolled sheet. The average cell density (cells per mm^2) was calculated by dividing the total cell count by the specimen area spanned by the image.

The 1- and 7-day specimens demonstrated similar average cell densities for actuated and non-actuated scaffolds. In some cases, the non-actuated specimens had a higher cell density than the actuated specimens, but the differences were small compared to the variations expected due to cell loss during unrolling tubes and other sources of fluctuation. However, for 10-, 14-, and 15-day specimens, a marked increase in the number of cells is found in the actuated scaffolds as compared to the non-actuated counterparts. The 10-day specimen showed a 33 times larger cell density compared to the non-actuated scaffold and the 14-day specimen showed a 69 times larger cell density. A second actuated 14-day test provided further corroboration of enhanced cell density, but the density could not be

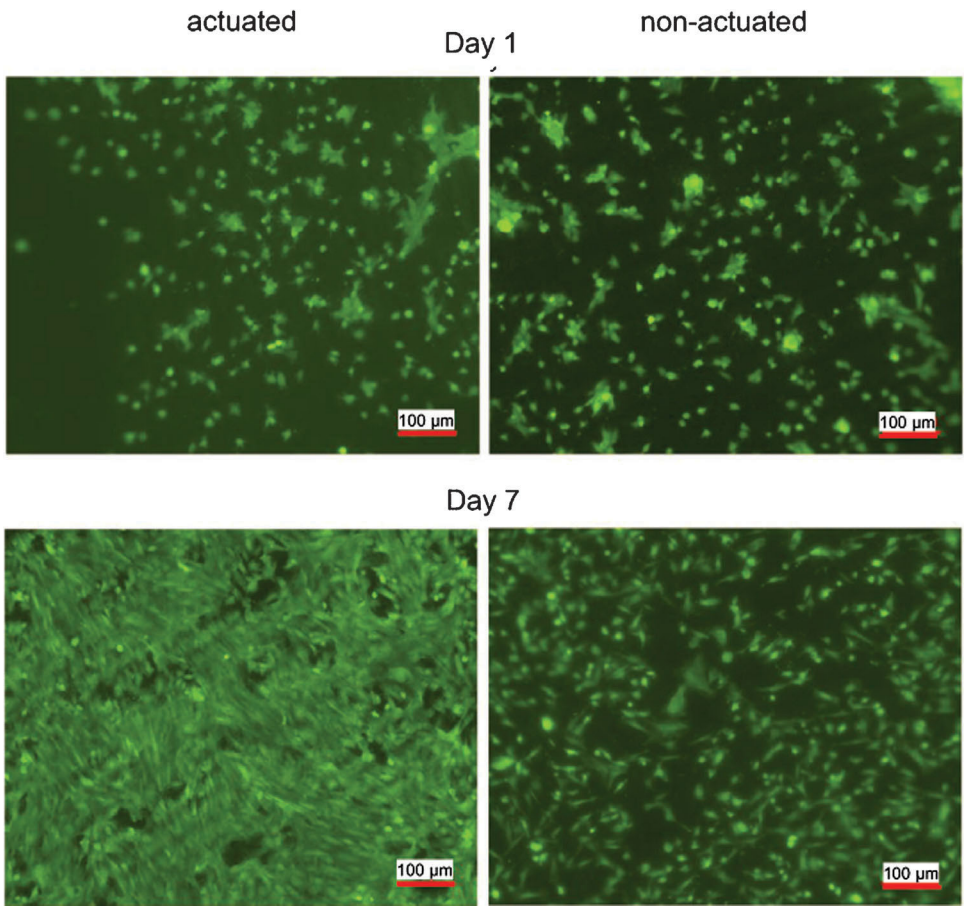

Figure 5. One hundred times optical micrographs of cells labeled with calcein-AM on unrolled sheets after 1 and 7 days of incubation. All images taken near mid-point of tube along its axis and mid-wall layer in tube wall.

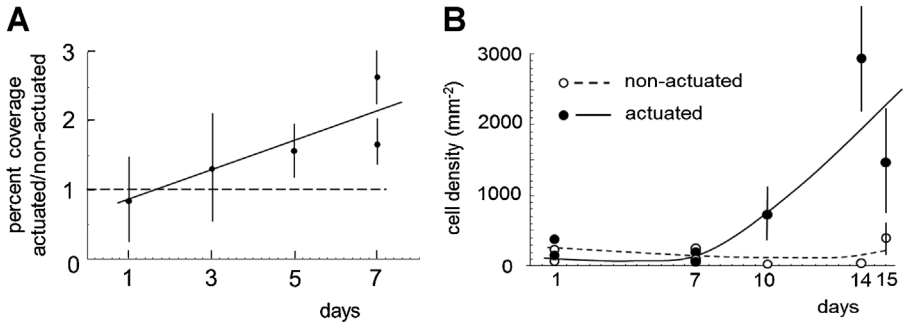

Figure 6. Cell densities found on unrolled tubes: **A**: trend in the ratio of the percent cell coverage seen for actuated specimens to that for non-actuated specimens deduced by threshold analysis of images of cells stained with calcein-AM; **B**: trend in the count per mm^2 of cell nuclei revealed by Hoescht-33342 staining for actuated and non-actuated specimens.

quantified because the tube could not be unrolled for examination, which could be associated to high production of ECM.

Complete data are presented for 15-day specimens in Tables E.1 and E.2 (see online material). The variation in cell density through the thickness of the wall was sampled near the middle of the tube's length. The density averaged through the wall thickness is approximately 4 times larger in the actuated scaffold than in the non-actuated scaffold. The density at the mid-wall location increases by a much greater factor, because the cell density in the actuated 15-day specimen peaks there whereas it is at a minimum there in the non-actuated specimen. Thus, the density in the mid-wall region of the 15-day actuated specimen is approximately 20 times higher than in the mid-wall region in the non-actuated specimen. The cell density at the mid-wall location is also maximum at the mid-span of the tube (zone I depicted in Fig. 3B), where the tube deflection is largest.

Trends in cell density using data from all specimens that were stained with Hoescht-33342 are shown in Figure 6B. Each datum is the average density determined from a series of images of an unrolled tube from its inside to its outside, at the mid-span of the tube's length. Error bars reflect the variance of deduced values from image to image within a series. Actuation has a significant effect for test durations beyond 7 days. Non-actuated specimens exhibit very low cell densities for durations of 10 and 14 days. The modest increase seen in the cell density for the non-actuated 15-day test is small and may not be significant. Of most significance is that the density averaged through the wall thickness for actuated tests of duration 10–15 days is one to two orders of magnitude greater than for non-actuated tests of the same duration.

Cell density data based on counting nuclei (Fig. 6B) are consistent with the trends inferred from percent coverage (Fig. 6A): modest increases are obtained by actuation for durations up to 7 days. The largest increases, both relative to

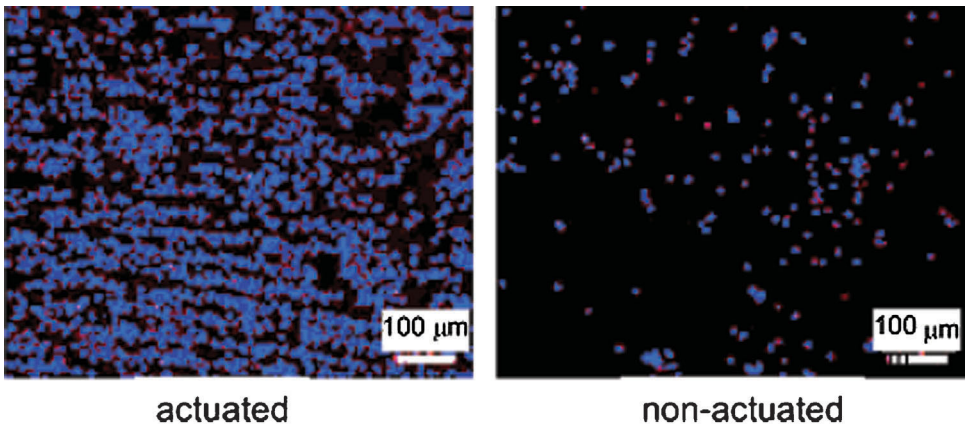

Figure 7. One hundred times optical micrographs of cells on unrolled sheets from a 15-day specimen, showing nuclei stained with Hoechst-33342. Images from mid-point along length of tube and mid-wall location within tube wall.

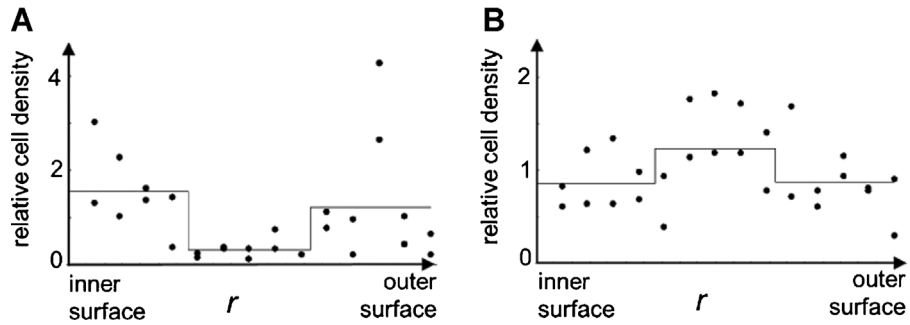

Figure 8. Variations in cell density through the thickness of the tube wall in combined data for 14- and 15-day specimens. Each density datum is normalized by the average density for that specimen. The fitted lines show the average of the normalized densities in the inner, middle, and outer third of the wall thickness. **A**: Non-actuated. **B**: Actuated.

the control and in absolute densities, are found between 10 and 15 days. Loss of cell density in non-actuated cases for durations greater than 7 days suggests starvation; continued proliferation in actuated cases implies that nutrition is maintained by the pumping caused by actuation.

The distribution of cells through the thickness of the tube wall shows interesting trends for the longer duration tests. Cell density data for 14- and 15-day tests are combined in Figure 8 by plotting each datum normalized by the average density for that specimen, thus emphasizing relative density variations with position, rather than absolute density values. For non-actuated specimens, the cell density is relatively low in the central third of the thickness of the wall (Fig. 8A), implying starvation of the interior cells due to limited diffusion. In contrast, the actuated specimens had the largest cell density in the central third of the wall thickness. The trend in Figure 8B implies a correlation between cell density and the amplitude of cyclic shear strains, which are also highest in the wall interior (see Fig. 4).

Collagen

The increased proliferation and clustering of cells in the magnetically actuated scaffolds raises the question of whether or not cells in the actuated scaffolds were producing a greater amount of extracellular matrix (ECM) compared to the control. Type-I collagen is one of the most abundant of the ECM proteins and has been shown to be synthesized by vascular SMC (Ponticos et al., 2004). Therefore, type-I collagen was selected as an indicator of ECM.

In a 15-day scaffold, green fluorescence from FITC (indicating the presence of type-I collagen) was observed concentrated in regions occupied by clusters or aggregates of cells as shown in Figure 9A and Supplementary Figure E.4. Lower magnification images of 14-day scaffolds show that collagen was widespread (see Fig. 9B). In non-actuated scaffolds, collagen production was zero or minimal (see Supplementary Figs. E.5 and E.6). For 10- and 14-day scaffolds, the collagen coverage was represented as the

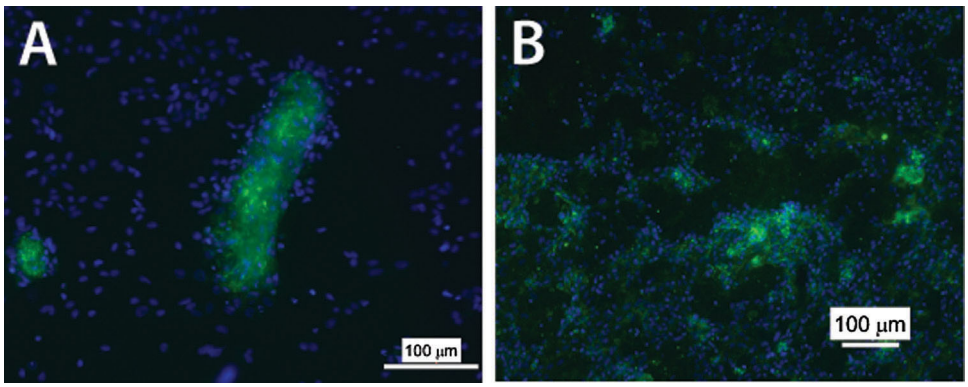

Figure 9. **A**: Cluster of cells observed in actuated 15-day specimen. blue = cell nuclei; green = collagen type I. **B**: Lower magnification image from actuated 14-day specimen shows widespread collagen type I.

percent of the image area that was above a threshold for FITC signal intensity. For non-actuated specimens, zero or insignificant amount of collagen was found, whereas for actuated specimens, collagen coverage ranged up to 10–35% (Tables II and III).

Discussion

Correlations With Strain and Nutrient Flux

Figure 8B suggests enhanced cell density in the mid-wall region (the interior of the tube wall), which correlates with the location of the largest shear strains. It does not correlate with nutrient pumping, which has uniform flux through the thickness of the wall. However, the low cell density in the mid-wall region in non-actuated specimens (Fig. 8A and Table E.2) implies that nutrient pumping is essential to avoiding cell death at the mid-wall region due to the sealing effect of cells proliferating at the surfaces.

Spatial Ordering

In some cultures actuated for 7 days or longer, images show a remarkable transition in the spatial ordering of the cells: they spontaneously organize themselves into rows. This organization is most easily seen in images in which the cell nuclei were stained (Fig. 7 and Supplementary Fig. E.3), but can also be discerned in the calcein-stained images for 5- and 7-day cultures (Fig. 5 and Supplementary Fig. E.1D and E). The row structure is evident almost exclusively in the images corresponding to the mid-wall region, but it is also present in one image corresponding to the inner surface of the tube (Supplementary Fig. E.1D). Correlation with the mid-wall location suggests that strain stimulus due to deformation of the tube scaffold, which peaks at the mid-wall location, is the most important factor, rather than fluid flow.

The images of nuclei reveal that each row is not a single line of cells, but a narrow band within which nuclei are distributed in space in an approximately statistically uniform manner. The calcein images reveal instances where the rows of cells are separated by gaps of zero intensity (e.g., Supplementary Fig. E.1D) and instances where the rows appear as brightness variations without gaps of zero intensity (Fig. 5). The spatial period of the rows varies between approximately 25 and 50 μm (Table IV), which is similar to the thickness of smooth muscle fibers in rats. The data do not suggest any systematic change in the period with the duration of incubation.

While unmistakable where it appears, organization of cells into rows is not universal; it did not appear in all actuated specimens. A possible explanation of this is that ordering into rows requires a particular range of strain amplitudes and strain rates to occur. Neither the strain amplitude nor the strain rate was closely controlled in the experiments reported here.

Table II. Percent collagen coverage for 10- and 14-day specimens.

	% image with threshold FITC signal	
10-day specimen	Non-actuated	Actuated
Left	0	0
...	0	0.06
...	0	4.13
...	0	1.51
...	0	0.35
Right	0	0.09

	% image with threshold FITC signal	
14-day specimen	Non-actuated	Actuated
Left	0	0
...	0	14.57
...	0	1.36
...	0.004	9.49
...	0	16.97
Right	0.007	0

Mid-wall region images were scanned from left to right along the length of the tube.

Table III. Percent collagen coverage for a 14-day specimen.

	% image with threshold FITC signal	
14-day specimen	Non-actuated	Actuated
Outer surface	0	No meas't
...	0	0.1
...	0	0.28
...	0	0.03
...	0	3.3
...	0	2.17
...	0	0.4
...	0	1.19
...	0	15.88
...	0.01	2.32
...	0.02	2.52
...	0.01	6.33
...	0	8.9
...	0.009	36.96
Inner surface	No meas't	39.14

Mid-tube images scanned from the outer to the inner surface through the thickness of the tube wall.

Future Developments

The fluid pressures achieved in the current study are a few percent or less of the pressure generated during natural

Table IV. Spacing (period) of rows of cells.

Culture reference	Period (mm)
7-day—#2	33 ± 2
7-day—#2	24 ± 2
7-day—#3	48 ± 2
15-day	37 ± 2

peristalsis of the intestine, approximately 10–100 mmHg or 1,200–12,000 Pa (Bray et al., 1999). If higher pressures were desired in another application, they could be achieved by a combination of increasing the wall thickness and increasing the magnetic field. For example, the wall thickness of natural intestine is 5–10 times greater than the wall thickness of the tube scaffolds studied here; while the magnetic field of a strong commercial electromagnet (e.g., for an MRI machine) or a permanent magnet with a dipole design is 10 times higher than the field used here, and the field in experimental electromagnets is 100 times higher (Craik, 1995; Jiles, 1991). Using strong commercial electromagnets and thick tube walls, pressures 100 times higher than those in the present study could be readily achieved, that is, $P \approx 3$ kPa or approximately 20 mmHg.

If a magnetically actuated tube is to be used in vivo as a scaffold for regenerating a section of intestine, for example, it will not be possible to plug its ends to prevent axial fluid flow. If axial flow is not limited, then the radial nutrient flow through the tube walls will not be achieved. However, limitation to axial flow will result naturally due to the viscous nature of the contents of the intestine. This viscosity will result in a characteristic time, τ_{axial}, for pressure loss due to axial flow, which will increase as the length of intestine subject to actuation increases. By actuating a sufficiently long section simultaneously, τ_{axial} can be made to exceed the characteristic time for flow of nutrient through the tube walls. Nutrient pumping will then be effective. Establishing values for τ_{axial}, and therefore for the minimum length of intestine that must be actuated, remains a topic for research. However, since electromagnets can generate spatially extensive fields, actuating long sections of intestine simultaneously could be achieved.

Conclusions

Magnetic actuation of a tube scaffold pumps nutrients through the walls of the tube and exerts strain stimuli upon resident cells. In non-actuated controls, cells in the interior of the walls of the tube begin to die with presumed lack of nutrient ingress. In contrast, for walls of the thickness studied (0.2 mm, including cells), evidence of nutrient deficiency is not found in actuated specimens: when pumping is effected by magnetic actuation, not only is cell death decreased in the wall interior but cell density is increased to values greater than at the tube wall exterior. Spatial variations of cell density through the thickness of the wall and along the length of the tube correlate with strain amplitude, implying that strain stimulus is a factor in enhanced growth rates.

The gain in cell density averaged through the wall thickness for actuated over non-actuated specimens ranges from 5–100 after 14–15 days. These summary numbers refer to the part of the tube scaffold that is directly above the actuating magnet, where the strain stimuli are strongest. In several actuated specimens, cells were observed to order themselves into rows. When it occurs, this spatial ordering also appears to correlate with locations of maximum shear strain. Finally, correlating with accelerated cell proliferation, substantial collagen type I production was evident in specimens actuated for 10–14 days. Negligible collagen appeared in non-actuated specimens.

The authors wish to thank Dr. Jennifer Andrew for providing magnetic nanoparticles. The content is solely the responsibility of the authors and does not necessarily represent the official views of the National Institute of Biomedical Imaging and Bioengineering or the National Institutes of Health.

References

Abousleiman RI, Sikavitsas VI. 2006. Bioreactors for tissues of the musculoskeletal system. Adv Exp Med Biol 585:243–259.

Asnaghi MA, Jungebluth P, Raimondi MT, Dickinson SC, Rees LEN, Go T, Cogan TA, Dodson A, Parnigott PP, Hollander AP, Birchall MA, Conconi MT, Macchiarini P, Mantero S. 2009. A double-chamber rotating bioreactor for the development of tissue-engineered hollow organs: From concept to clinical trial. Biomaterials 30:5260–5269.

Bray JJCP, MacKnight ADC, Mills RG. 1999. Lecture notes on human physiology, 4th edn. Hoboken, New Jersey: Blackwell.

Carrier RL, Rupnick M, Langer R, Schoen FJ, Freed LE, Vunjak-Novakovic G. 2002. Perfusion improves tissue architecture of engineered cardiac muscle. Tissue Eng 8:175–188.

Craik DJ. 1995. Magnetism: Principles and applications. Chichester: John Wiley & Sons.

Dennis RG, Smith B, Philp A, Donnelly D, Baar K. 2009. Bioreactors for guiding muscle tissue growth and development. Adv Biochem Eng Biotechnol 112:39–79.

Derfus AM, von Maltzahn G, Harris TJ, Duza T, Vecchio KS, Ruoslahti E, Bhatia SN. 2007. Remotely triggered release from magnetic nanoparticles. Adv Mater 19:3932–3936.

Freed LE, Guilak F, Guo XE, Gray M, Tranquillo R, Holmes JW, Radisic M, Sefton MV, Kaplan D, Vunjak-Novakovic G. 2006. Advanced tools for tissue engineering: Scaffolds, bioreactors, and signaling. Tissue Eng 12:3285–3305.

Galban CJ, Locke BR. 1999. Analysis of cell growth kinetics and substrate diffusion in a polymer scaffold. Biotechnol Bioeng 65:121–132.

Griffith LG, Naughton G. 2004. Tissue engineering—Current challenges and expanding opportunities. Science 295:1009–1014.

Hoare T, Santamaria J, Goya GF, Irusta S, Lin D, Lau S, Padera R, Langer R, Kohane DS. 2009. A magnetically-triggered composite membrane for on-demand drug delivery. Nano Lett 14:3651–3657.

Ishaug-Riley SL, Crane-Kruger GM, Yaszemski MJ, Mikos AG. 1998. Three-dimensional culture of rat calvarial osteoblasts in porous biodegradable polymers. Biomaterials 19:1405–1412.

Jiles D. 1991. Introduction to magnetism and magnetic materials. London: Chapman and Hall.

Lee M, Wu BM, Dunn JC. 2008. Effect of scaffold architecture and pore size on smooth muscle cell growth. J Biomed Mater Res A 87:1010–1016.

Mack JJ, Cox BN, Sudre O, Corrin AA, Lucato SL, Ma C, Andrew JS. 2009. Achieving nutrient pumping and strain stimulus by magnetic actuation of tubular scaffolds. Smart Mater Struct 18:104025–104040.

Nikles SM, Nikles J, Hudson J, Nikles DE. 2010. Diblock copolymers for magnetically triggered drug delivery system. Joshua 7:35–39.

Ponticos M, Partridge T, Black CM, Abraham DJ, Bou-Gharios G. 2004. Regulation of collagen type I in vascular smooth muscle cells by competition between Nkx2.5 and deltaEF1/ZEB1. Mol Cell Biol 24:6151–6161.

Shieh S-J, Vacanti JP. 2005. State-of-the-art tissue engineering: From tissue engineering to organ building. Surger 137:1–7.

Sikavitsas VI, Bancroft GN, Lemoine JJ, Liebschner MAK, Dauner M, Mikos AG. 2005. Flow perfusion enhances the calcified matrix deposition of marrow stromal cells in biodegradable nonwoven fiber mesh scaffolds. Ann Biomed Eng 33:63–70.

Tandon N, Marsano A, Maidhof R, Numata K, Montouri-Sorrentino C, Cannizzaro C, Voldman J, Vunjak-Novakovic G. 2010. Surface-patterned electrode electrode bioreactor for electrical stimulation. Lab Chip 10:692–700.

Tandon N, Marsano A, Maidhof R, Wan L, Park H, Vunjak-Novakovic G. 2011. Optimization of electrical stimulation parameters for cardiac tissue engineering. J Tissue Engin Regen Med 5:e115–e125.

Timoshenko SP, Goodier JN. 1970. Theory of elasticity, 3rd edn. New York: McGraw-Hill.

Volkmer E, Drosse I, Otto S, Stangelmayer A, Stengele M, Kallukalam BC, Mutschler W, Scheiker M. 2008. Hypoxia in static and dynamic 3D culture systems for tissue engineering of bone. Tissue Eng A 14:1331–1340.